JEB™
Website : www.jeb.co.in
E-mail : editor@jeb.co.in

Journal of Environmental Biology

ISSN: 0254-8704 (Print)
ISSN: 2394-0379 (Online)
CODEN: JEBIDP

Hydrodynamic analysis of rigid and flexible pectoral fins

Ningyu Li[1]*, Yumin Su[1], Zhaoli Wang[2], Weixing Liu[1], Muhammad Aqeel Ashraf[3] and Zhiyang Zhang[4]

[1]Science and Technology on Underwater Vehicle Laboratory, Harbin Engineering University, Harbin-150 001, China

[2]Beijing Institute of Control Engineering, Beijing-100 190, China

[3]Faculty of Science and Natural Resources, University Malaysia Sabah-88400 Kota Kinabalu, Sabah, Malaysia

[4]Deepwater Engineering Research Center, Harbin Engineering University, Harbin-150 001, China

*Corresponding Author E-mail: **liningyu123@aliyun.com**

Publication Info

Paper received:
05 March 2016

Revised received:
27 April 2016

Re-revised received:
5 May 2016

Accepted:
23 June 2016

Abstract

Numerical study on unsteady hydrodynamic characteristics of rigid and flexible pectoral fins in viscous flow-field was performed in the present study. The effect of key kinematical parameters on the propulsion performance was analyzed. The propulsion mechanism was explored by evolution of wake vortices. Computational results revealed that optimal combination for investigated parameters was $U = 4C$, $\phi_{FLA} = 45^{\circ}$, $\Delta\phi_{FL} = 60^{\circ}$ and $a_0 = 0.2$. Wake vortices were shed from two edges of fin and fin tip and convect downstream as well as laterally. For flexible pectoral fin, the shedding time was delayed and shed wake vortices keep longer time near the fin that led to difference in variation amplitude of hydrodynamics as compared to rigid fin. The hydrodynamic performance of flexible fin was superior to that of rigid fin for low incoming velocity. However, the opposite situation occured for high incoming velocity.

Key words

CFD, Flexible body, Hydrodynamics, Pectoral fin, Wake vortex

Introduction

In future, bionic Unmanned Underwater Vehicle (UUV) will be used for spreading military equipment and ocean developing field. On bionic UUV, caudal fin was used for propulsion. However, only with the help of pectoral fin, agile maneuver and arbitrary gesture-control was achieved on bionic UUV. Many fish finish maneuver such as suspension, forward movement and backward movement by motion of pectoral fin. Research on bionic pectoral fin propulsion has been a focus of considerable theoretical, numerical and experimental work.

Gibb *et al.* (1994) reported that pectoral fins of ray-finned fish usually undergo a compound motion rather than a clear rolling motion or pitch motion. Westneat and Walker (1997) also drawn similar conclusions. Drucker and Lauder (1999) analyzed the movement and flow field of pectoral fin according to qualitative observation by use of Digital Particle Image Velocimetry (DPIV) technology and measured the force of pectoral fin. Kato (1984, 1996, 1998-2000 and 2004) studied the hydrodynamic performance of bass-like mechanical pectoral fin based on numerical and experimental method and the hydrodynamic analysis of flexible multi-fins was carried out with the application of pectoral fin motion mode to bionic UUV. Wang *et al.* (2010) studied the hydrodynamic performance of a pectoral fin propulsive system experimentally and numerically where some parameters were changed.

In the present study, the propulsion mechanism of rigid and flexible pectoral fins were studied by numerical modeling. This was completely different from previous investigations, as attention was focused not only on the fin

hydrodynamic performance but also on the corresponding wake vortices. The effect of incoming velocity, flapping amplitude, phase angle between flapping and lead-lag and flexure amplitude on the propulsion performance was analyzed. Comparison of hydrodynamic performance and wake structure between rigid and flexible fins were performed.

Materials and Methods

Computational model : Modeled from the observed pectoral fin of the bass, the pectoral fin used in the numerical simulation is shown in Fig. 1. The maximum chord length C and span length L were 0.155m and 0.188m, respectively. The incoming velocity U was uniform. The coordinate system is shown in Fig. 2. The inertial reference frame O - XYZ and the moving reference frame G - $X_G Y_G Z_G$ were defined accordingly. Based on the summary of motion law of pectoral fin (Azuma, 1992) and the observations from the experiment (Drucker and Lauder, 1999), the numerical simulation was conducted with cosine motion models and applied for lead-lag, feathering and flapping motions. The frequency of the above three motion were same. The lead-lag motion of the pectoral fin is defined as :

$$\phi_L = \phi_{LC} - \phi_{LA} \cdot \cos(2\pi f t) \quad (1)$$

where, ϕ_{LC} is the average angle of lead-lag motion; ϕ_{LA} is the lead-lag amplitude; f is the motion frequency of pectoral fin and t is the time.

The feathering motion of pectoral fin was defined as:

$$\phi_{FE} = -\phi_{FEC} - \phi_{FEA} \cdot \cos(2\pi f t + \Delta\phi_{FE}) \quad (2)$$

where, ϕ_{FEC} is the average angle of feathering motion; ϕ_{FEA} is the feathering amplitude and $\Delta\phi_{FE}$ is the phase angle between feathering and lead-lag.

The flapping motion of pectoral fin was defined as:

$$\phi_{FL} = \phi_{FLC} + \phi_{FLA} \cdot \cos(2\pi f t + \Delta\phi_{FL}) \quad (3)$$

where, ϕ_{FLC} is the average angle of flapping motion; ϕ_{FLA} is the flapping amplitude, and $\Delta\phi_{FL}$ is the phase angle between flapping and lead-lag.

The dimensionless frequency was defined as:

$$k = C \cdot 2\pi f / U \quad (4)$$

According to the above analysis and the coordinate system, the definition of hydrodynamic and moment coefficients are as follows:

$$\begin{cases} C_x = \dfrac{F_x}{0.5 \cdot \rho U^2 S} \\ C_y = \dfrac{F_y}{0.5 \cdot \rho U^2 S} \\ C_z = \dfrac{F_z}{0.5 \cdot \rho U^2 S} \end{cases} \quad (5)$$

where, ρ is the fluid density; S is the surface area of pectoral fin and F_x, F_y and F_z are the thrust, lateral force and lift, respectively.

The average thrust, lateral force and lift coefficients were defined as :

$$\begin{cases} C_{xm} = \dfrac{1}{T}\int_0^T C_x dt \\ C_{ym} = \dfrac{1}{T}\int_0^T C_y dt \\ C_{zm} = \dfrac{1}{T}\int_0^T C_z dt \end{cases} \quad (6)$$

where, T is the motion period.

The efficiency of pectoral fin was defined as:

$$\eta = \overline{P}_{out} / \overline{P}_{in} \quad (7)$$

where, $\overline{P}_{out}$ is the average power output during one period and $\overline{P}_{in}$ is the average power input during one period.

$$\overline{P}_{out} = C_{xm} U \quad (8)$$

$$\overline{P}_{in} = -\frac{1}{T}\int_0^T \int_{A_{FIN}} (\vec{\sigma} \cdot \vec{V}) dA dt \quad (9)$$

where, A_{FIN} denotes the fin surface $\vec{\sigma}$ is the surface force and $\vec{V}$ is the local velocity of fin surface.

Numerical Method

Mesh generation: In order to effectively predict the hydrodynamic performance, dynamic mesh technique in FLUENT was used to simulate the unsteady flow field induced by pectoral fin. For the purpose of accurate simulation of developing boundary layer flow on the pectoral fin, the current study adopts the unstructured mesh. Additionally, the overall computational domain was divided into one kernel area and six non-kernel areas.

Fig. 3 shows the mesh around the pectoral fin. Following grid refinement studies, the kernel area and each non-kernel area was covered by 600000 and 100000 unstructured cells respectively, which were used to encompass the entire pectoral fin.

CFD technology : The unsteady viscous flow-field around the pectoral fin was computed by solving Reynolds Averaged Navier-Stokes (RANS) equations with unstructured grids. The simulations employed a finite-volume method by using commercial CFD software FLUENT. Therefore, continuity and momentum equations (Zhang *et al.,* 2012) were described as:

$$\frac{\partial \rho}{\partial t} + \frac{\partial}{\partial x_i}(\rho u_i) = 0 \tag{10}$$

$$\frac{\partial(\rho u_i)}{\partial t} + \frac{\partial}{\partial x_j}(\rho u_i u_j) = -\frac{\partial p}{\partial x_i} + \frac{\partial}{\partial x_j}(\mu \frac{\partial u_i}{\partial x_j} - \rho \overline{u_i' u_j'}) + S_i (i, j = 1, 2, 3) \tag{11}$$

where, μ is the molecular viscosity coefficient; u_i is the transient velocity component, u' is the fluctuating velocity component; u_i is the mean velocity component and S_i is the source item.

The shear-stress transport (SST) k-omega model (Wang *et al.,* 2009) was applied for the effect of turbulence. Since the instantaneous flow velocity on the fin in the computational domain must be equal to the local surface velocity, it was described by the motion of pectoral fin. A no-slip boundary condition was imposed on the fin surface and the motion of the pectoral fin was realized by UDF program (FLUENT Inc, 2006). Meanwhile, inflow boundary conditions were imposed on the front boundary faces. Free stream velocity conditions were specified at the outflow boundary.

Results and Discussion

Validation of calculation method : In order to verify the numerical method, first the pectoral fin in two degree of freedom (dof) motion was calculated. The numerical results were compared with the experimental and numerical results by Kato (1999). The Unsteady Vortex Lattice Method (UVLM) (Su *et al.,* 2007) was also adopted to verify the CFD technology.

With the parameters of $\phi_{LC} = 35^\circ$, $\phi_{FEC} = 35^\circ$, $\phi_{LA} = 35^\circ$, $\phi_{FEA} = 35^\circ$, $\phi_{FLC} = 0^\circ$, $\phi_{FLA} = 0^\circ$, $k = 4$, $\Delta\phi_{FE} = 60^\circ$ and $\Delta\phi_{FL} = 0^\circ$, comparison of the results from FLUENT, UVLM and experimental and numerical results by Kato (1999) are shown in Fig. 4.

From these, it can be seen that the changing trends of calculation results of FLUENT and UVLM were consistent

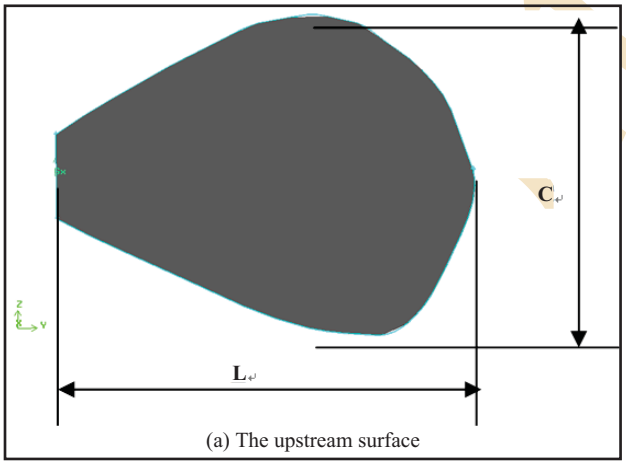

(a) The upstream surface

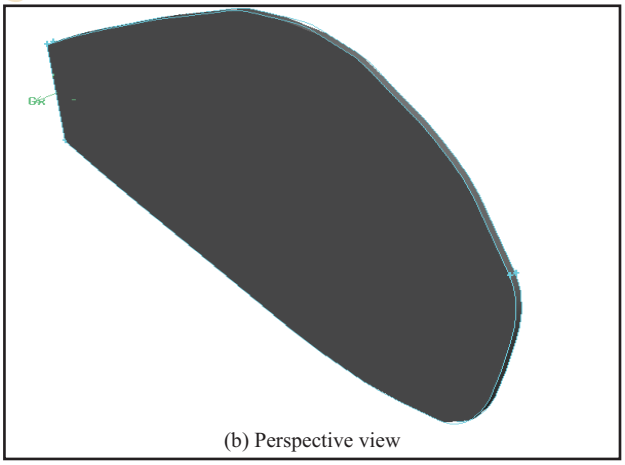

(b) Perspective view

Fig.1 : Pectoral fin

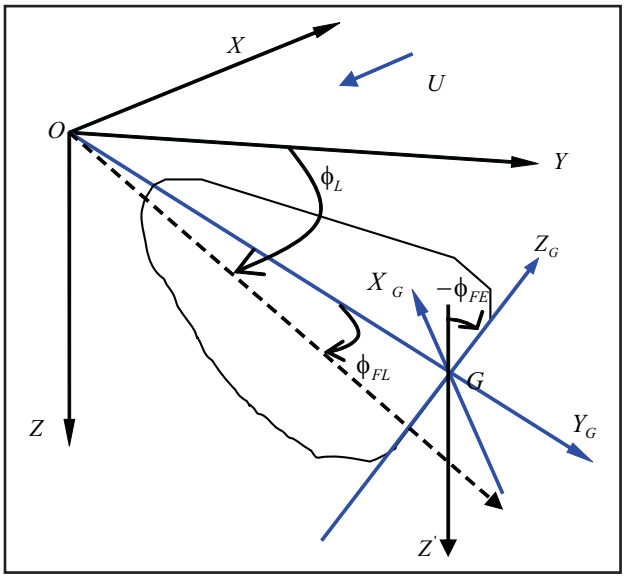

Fig. 2 : Reference frame

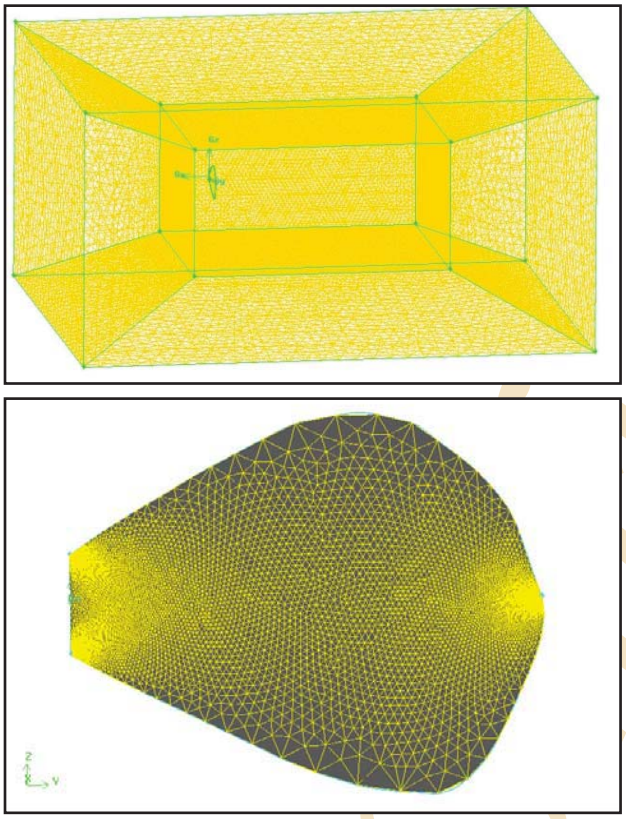

Fig. 3 : Mesh model of the pectoral fin

with the experimental and numerical results by Kato (1999). The viscosity and thickness of pectoral fin were considered in the CFD method, so the numerical method adopted in the present study calculate the hydrodynamic performance of pectoral fin in the real environment better than the UVLM.

After this the pectoral fin in 3-dof motion was calculated to further check the validation of calculation method. The calculation conditions were $\phi_{LC}=35^{\circ}$, $\phi_{FEC}=35^{\circ}$, $\phi_{LA}=35^{\circ}$, $\phi_{FEA}=35^{\circ}$, $\phi_{FLC}=35^{\circ}$, $\phi_{FLA}=35^{\circ}$, $k=4$, $\Delta\phi_{FE}=60^{\circ}$ and $\Delta\phi_{FL}=60^{\circ}$. In Fig. 5, the calculation results from FLUENT were compared with the numerical results of UVLM. The comparison showed that the changing trend of two calculations were mostly consistent, in spite of being partly different for the thrust coefficient during the period of second half period. The reasons for the difference were probably that the thickness of pectoral fin was not considered in the UVLM and the basic principles in two computational methods were different.

On comparing Fig. 4 and Fig. 5, it was seen that the CFD method adopted in the present study was validated to simulate the hydrodynamic performance of pectoral fin in unsteady motion.

Hydrodynamic analysis of rigid pectoral fin with different parameters:

Incoming velocity : Fig. 6 shows the hydrodynamic performance of pectoral fin with increase in the incoming velocity in case of $\phi_{LC}=\phi_{LA}=\phi_{FLC}=\phi_{FLA}=\phi_{LC}=35^{\circ}$, $\phi_{FEC}=\phi_{FEA}=45^{\circ}$, $\Delta\phi_{FE}=\Delta\phi_{FL}=60^{\circ}$ and $f=0.4$ Hz. The range of incoming velocity for computation was $U=1C\sim9C$.

Fig. 6, shows that C_{xm} rapidly decreased with increase in the incoming velocity in case of incoming flow at a speed smaller than $4C$ and then the trend of decreasing became slower as the speed increased. When velocity increased to $9C$, the thrust became negative. The peak point of efficiency curve emerged when the incoming velocity was $4C$. In the next numerical calculations, the incoming velocity was selected as $4C$.

Flapping amplitude : The range of flapping amplitude for computation was $\phi_{FLA}=15^{\circ}$-55° and ϕ_{FLC} was same as ϕ_{FLA}. The other parameters for numerical simulations were $U=4C$, $\phi_{LC}=\phi_{LA}=35^{\circ}$, $\phi_{FEC}=\phi_{FEA}=45^{\circ}$, $\Delta\phi_{FE}=\Delta\phi_{FL}=60^{\circ}$ and $f=0.4$ Hz.

The numerical results are shown in Fig. 7. It was seen that C_{xm} decreased at first until ϕ_{FLA} approached 25° and then it increased and showed a peak point at $\phi_{FLA}=45^{\circ}$. When ϕ_{FLA} was between 45° and 50°, C_{xm} decreased again and finally it increased again, but the value was not large enough. η decreased with increase in ϕ_{FLA} at first until it approached 20° and then it increased and reached maximum value at $\phi_{FLA}=$

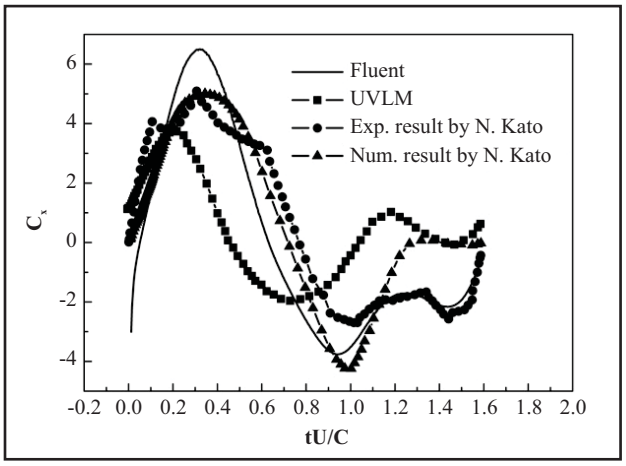

(a) Thrust coefficient

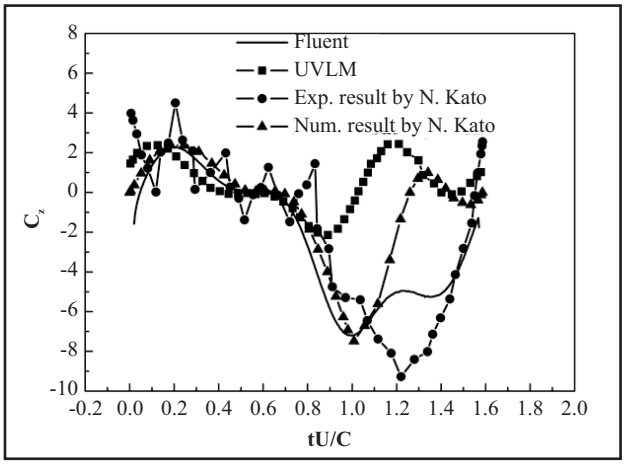

(b) Lift coefficient

Fig. 4 : Comparison of hydrodynamic coefficients during one period

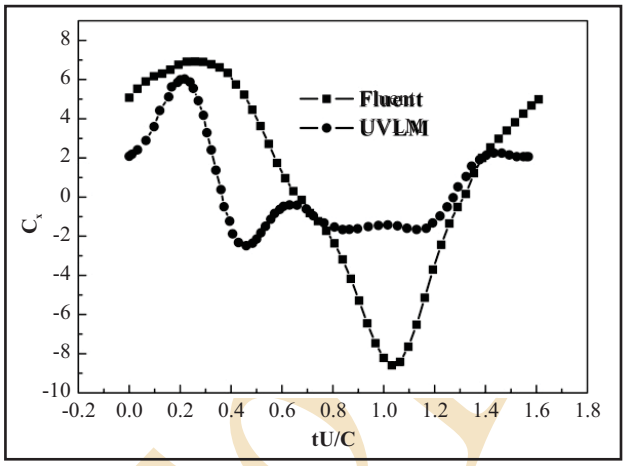

(a) Thrust coefficient

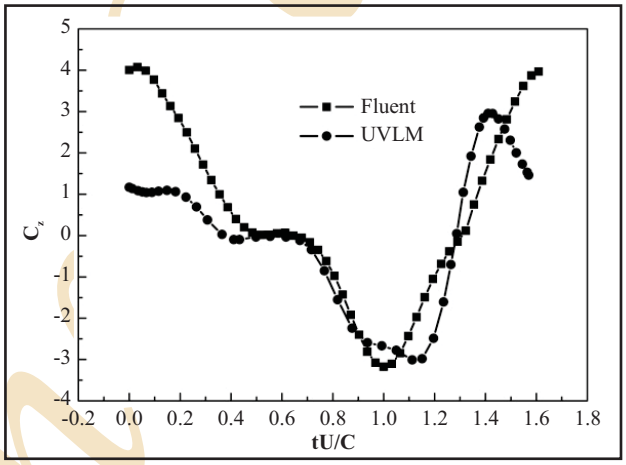

(b) Lift coefficient

Fig. 5 : Calculation result with two different method

45°, and finally decreased again. From the above discussion, it can be deduced that the optimal flapping amplitude was 45°.

Phase angle between flapping and lead-lag : In this section, the impact of phase angle between flapping and lead-lag on the hydrodynamic performance was studied. With the parameters of $U = 4C$, $\phi_{LC} = \phi_{LA} = 35^\circ$, $\phi_{FEA} = \phi_{FEC} = \phi_{FLC} = \phi_{FLA} = 45^\circ$, $\Delta\phi_{FE} = 60^\circ$ and $f = 0.4$ Hz, the average thrust coefficient and efficiency are shown in Fig. 8 for different phase angle between flapping and lead-lag $\Delta\phi_{FL} = 0^\circ$ - 180°.

For average thrust coefficient C_{xm}, with increase in $\Delta\phi_{FL}$, it increased in the case of $\Delta\phi_{FL}$ at a value smaller than 60° and rapidly decreased until $\Delta\phi_{FL}$ was 90° when the minimum occurs, finally it increases again. As $\Delta\phi_{FL}$ increased, η increased at first and showed a peak point at $\Delta\phi_{FL} = 60^\circ$ and after that it rapidly decreased until $\Delta\phi_{FL} = 90^\circ$. When $\Delta\phi_{FL}$ was between 90° and $\Delta\phi_{FL}$ = 0° - 120°, η increased and finally decreased. Based on the above analyses, the case of $\Delta\phi_{FL} = 90^\circ$ should be avoided and the optimal $\Delta\phi_{FL}$ is 60°.

Study of the propulsion mechanism of rigid pectoral fin : The propulsion mechanism can be analyzed by the evolution of wake vortices. Hydrodynamic characteristics can also be studied. Since it is very difficult to capture and display the three-dimensional vortex topology, the vorticity contours were intercepted on the surfaces that were parallel to the YOZ, XOZ and XOY plane respectively to show the corresponding vortex wake. In the following section Wx, Wy and Wz denote wake vortices on the surfaces that were parallel to YOZ, XOZ and XOY plane respectively.

On the basis of the analysis in section 4.2, the selected parameters for study of the propulsion mechanism of the pectoral fin are as follows : $U = 4C$, $\phi_{LC} = \phi_{LA} = 35^\circ$, $\phi_{FEA} = \phi_{FEC} =$

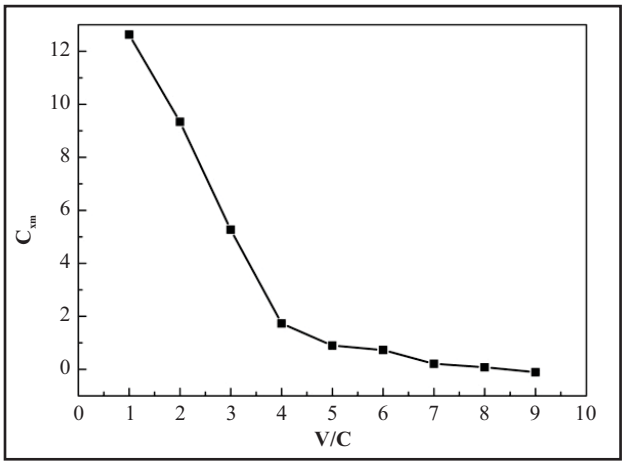

(a) Average thrust coefficient

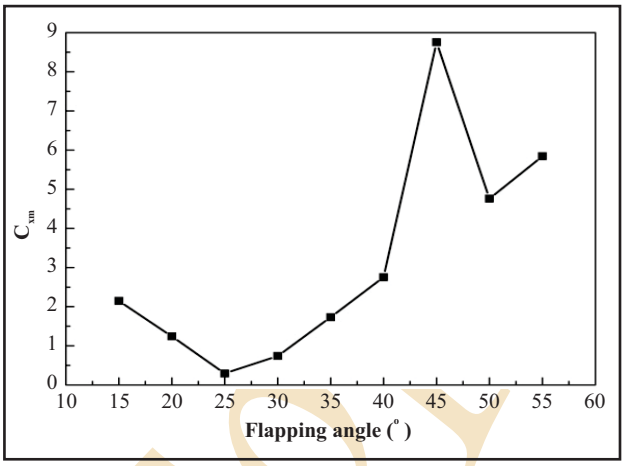

(a) Average thrust coefficient

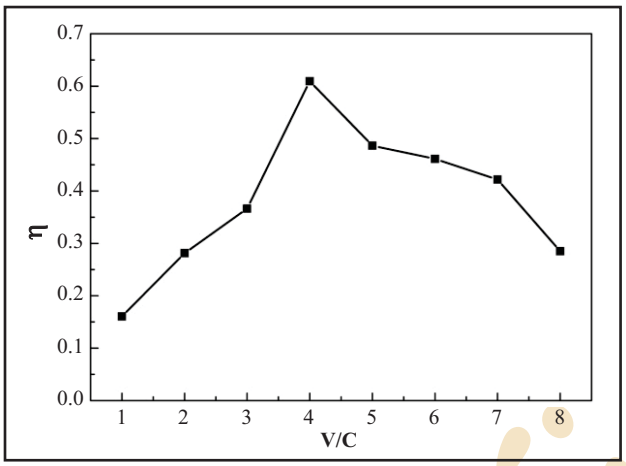

(b) Efficiency

Fig. 6 : Hydrodynamic performance with the incoming velocity

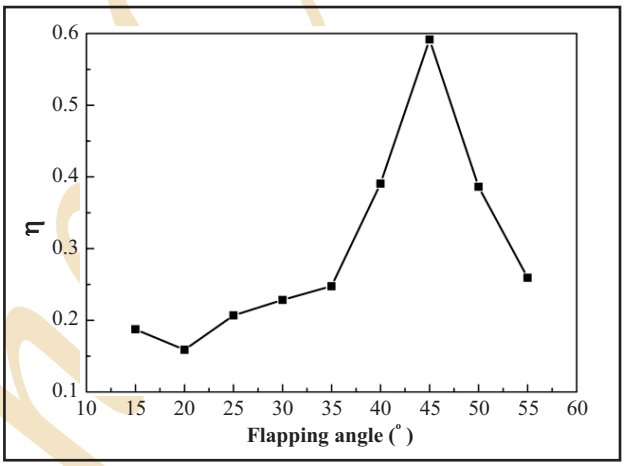

(b) Efficiency

Fig. 7 : Hydrodynamic performance with the flapping motion amplitude

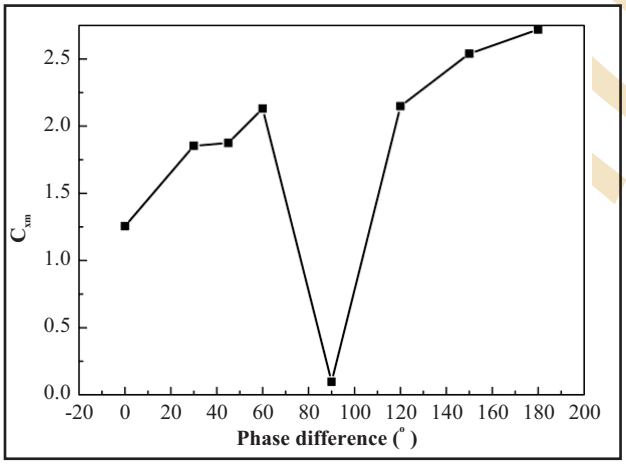

(a) Average thrust coefficient

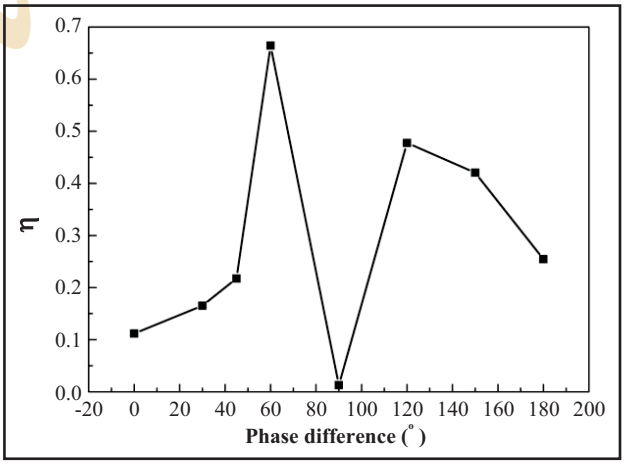

(b) Efficiency

Fig. 8 : Hydrodynamic performance with the phase angle between flapping and lead-lag

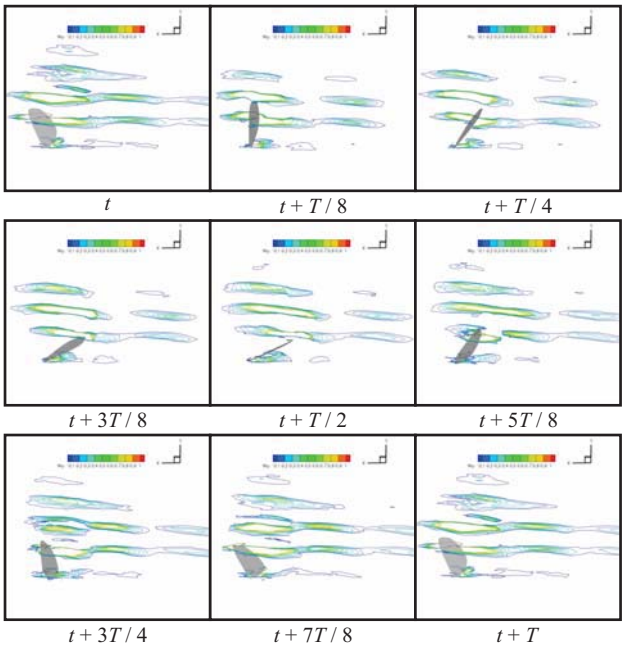

Fig. 9 : Vortical pattern visualized in 3-dof motion of the rigid pectoral fin from y direction

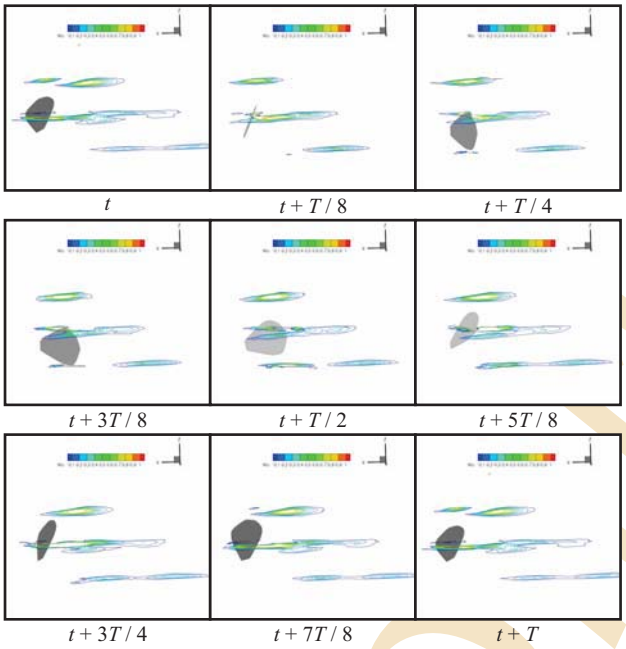

Fig. 10 : Vortical pattern visualized in 3-dof motion of rigid pectoral fin from z direction

$\phi_{FLC} = \phi_{FLA} = 45^{\circ}$, $\Delta\phi_{FE} = \Delta\phi_{FL} = 60^{\circ}$ and $f = 0.4$ Hz. Fig. 9, 10 and 11 shows the evolution of Wy, Wz and Wx for one period, respectively.

From Fig. 9, it is evident that during the motion of pectoral fin, Wy was shed from two edges of fin and fin tip that convects downstream and laterally. Wake vortices were

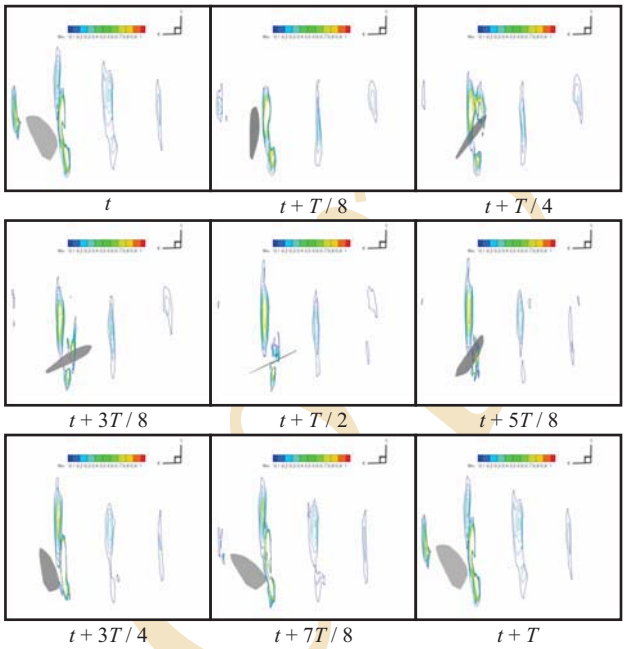

Fig. 11 : Vortical pattern visualized in 3-dof motion of rigid pectoral fin from *x* direction

separated from each other in each shedding direction and the interaction among them was weak. As shown in Fig. 10, primarily Wz was shed and it experienced the viscous dissipation downstream. Additionally, these wake vortices separated from each other in the shedding direction with weak interaction. From Fig. 11, Wx was shed from two edges of the fin and fin tip that convect downstream and laterally. In *x* direction, wake vortices were separated from each other and interaction among them was weak. However, in *y* direction the motion velocity of pectoral fin was faster than the shedding velocity. So wake vortices were divided by the pectoral fin at a certain moment, a little earlier than *T*/4 with the increase in the vorticity magnitude and the phenomenon lasted until a certain moment a little earlier than 3*T*/4.

The hydrodynamic coefficients during one period are shown in Fig. 12. According to Fig. 9-12 and the above analysis we can explain the relation between wake vortices and hydrodynamics to understand the propulsion mechanism of the pectoral fin. At the beginning of motion period, the first wake vortex was formed along the edge of pectoral fin and was shed into the wake with lead-lag motion. Due to feathering and flapping motions, the strength of wake vortex increased. The thrust, the lateral force and lift increased under the influence of wake vortex. The phenomenon lasted until a certain moment a little earlier than *T*/4. After the shedding of the first wake vortex, the second wake vortex was formed and developed gradually on the surface of the fin. Under the

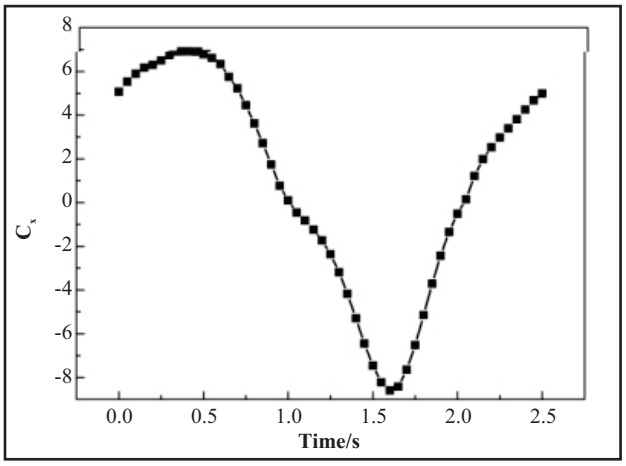

(a) Thrust coefficient

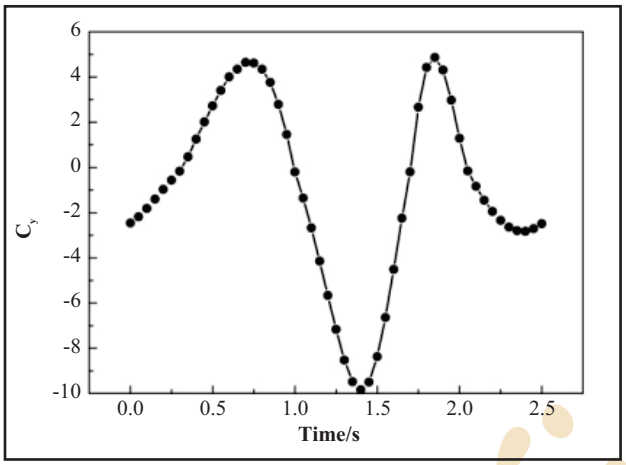

(b) Lateral force coefficient

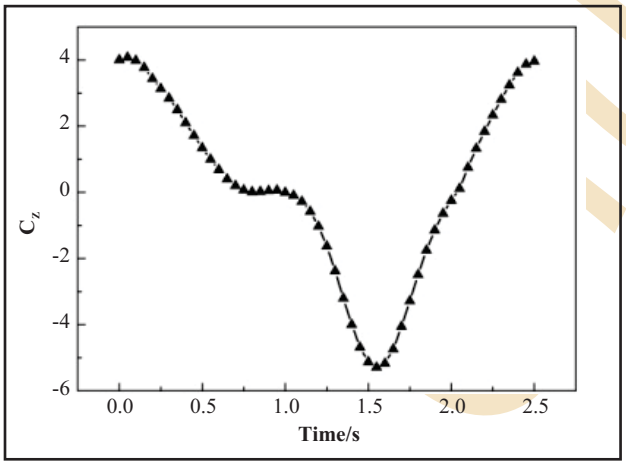

(c) Lift coefficient

Fig. 12 : Hydrodynamic coefficients in 3-dof motion of rigid pectoral fin during one period

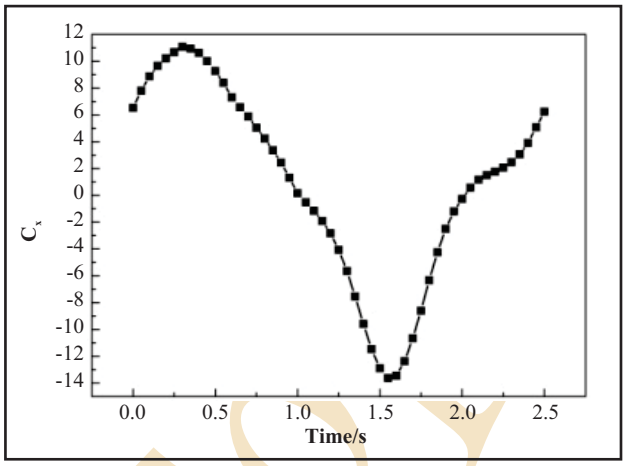

(a) Thrust coefficient

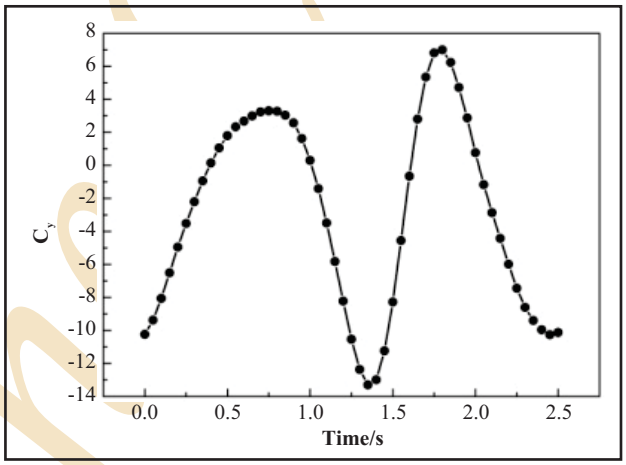

(b) Lateral force coefficient

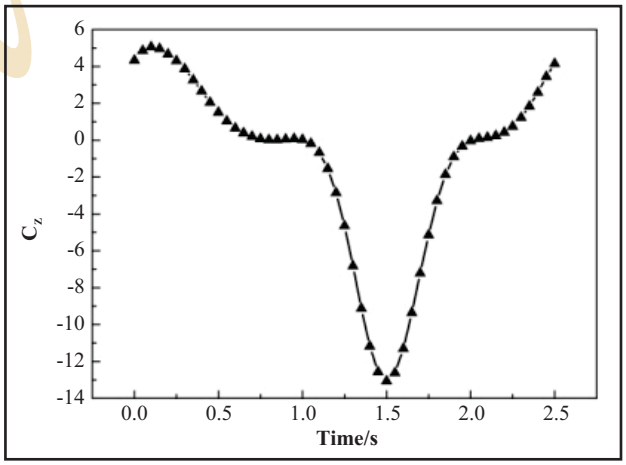

(c) Lift coefficient

Fig. 13 : Hydrodynamic coefficients in 3-dof motion of flexible pectoral fin during one period

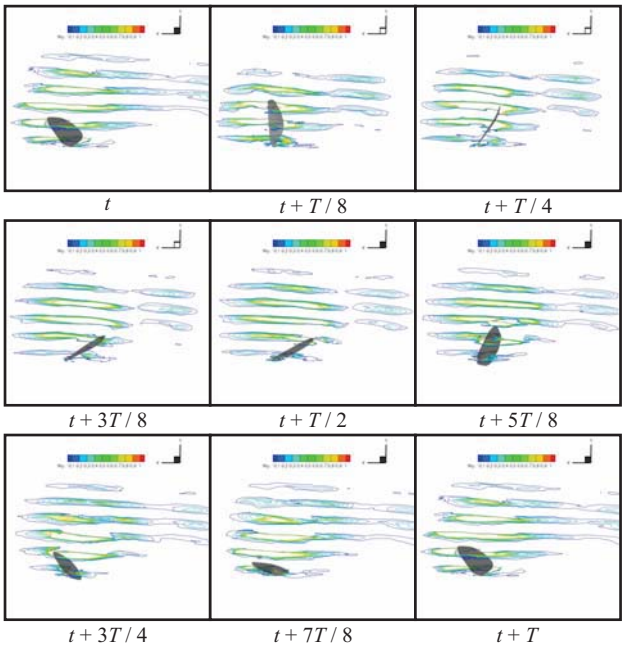

Fig. 14 : Vortical pattern visualized in 3-dof motion of the flexible pectoral fin from y direction

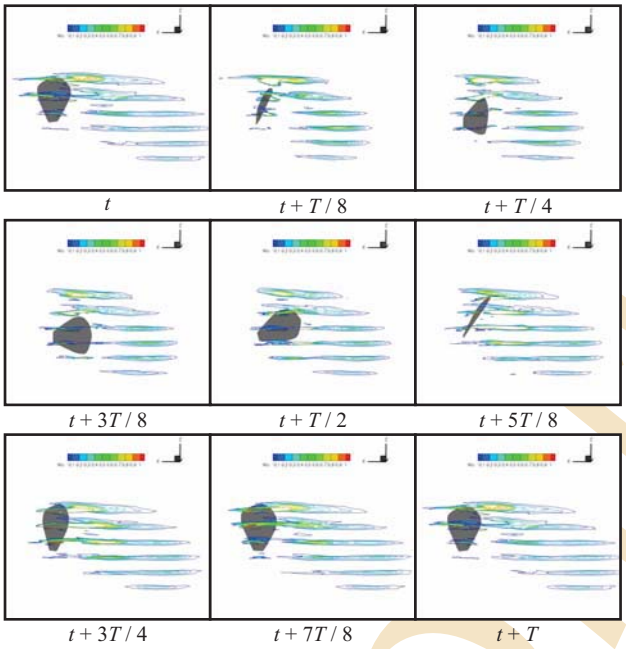

Fig. 15 : Vortical pattern visualized in 3-dof motion of the flexible pectoral fin from *z* direction

impact of wake vortex, the thrust decreased. As the wake vortex was shed into the wake, the thrust was further decreased. The phenomenon lasted until the second wake vortex was shed. The new wake vortex which was formed and grew gradually on the surface of the fin led to the increase in thrust.

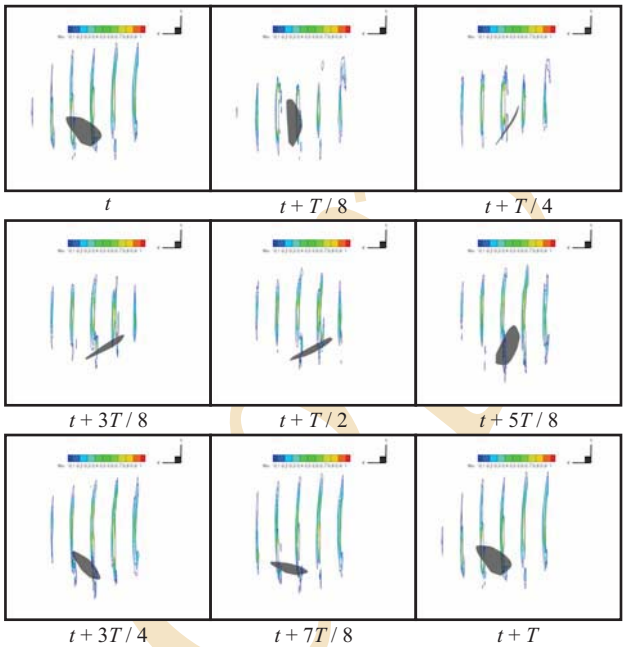

Fig. 16 : Vortical pattern visualized in 3-dof motion of the flexible pectoral fin from *x* direction

Owing to the periodicity variation of formation and shedding of wake vortex near the fin, twice periodicity variations of thrust occured during one period. Under the influence of flapping motion, especially during the second half period, the lateral force showed two peak points during one period. The presence of flapping motion led to stronger lift reflection.

Flexible pectoral fin : In addition to the above simulations on the rigid pectoral fin, additional simulations on the flexible pectoral fin were carried out in order to assess the effect of the flexibility.

Deformation mode : Considering the special motion mode of the pectoral fin, based on the previous theoretical and experimental study on the flexible pectoral fin, spanwise deformation was added to the calculation model of the rigid pectoral fin to set up the calculation model of flexible pectoral fin. The deformation profile for the moving reference frame is formulated follows :

$$x = a_0 / L \cdot \cos(2\pi ft) \quad (12)$$

where, a_0 is the flexure amplitude.

Study of the propulsion mechanism of flexible pectoral fin : The selected parameters for the study of the propulsion mechanism of the flexible pectoral fin are as follows : $U = 4C$,

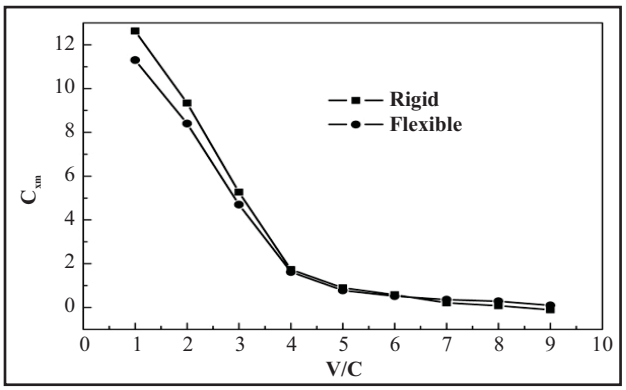

(a) Average thrust coefficient

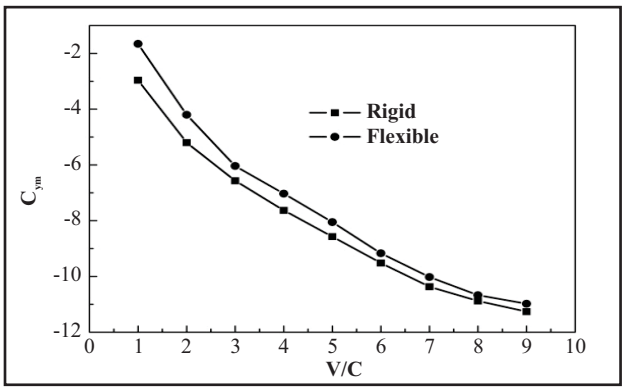

(b) Average lateral force coefficient

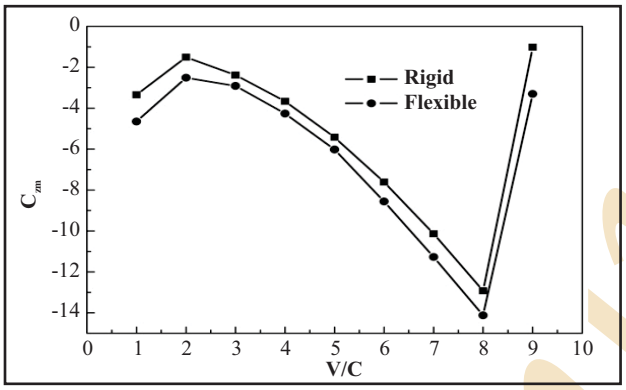

(c) Average lift coefficient

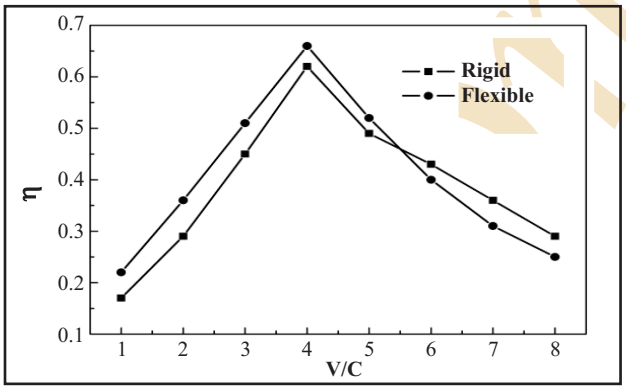

(d) Efficiency

Fig. 17 : Hydrodynamic performance for rigid and flexible pectoral fins with different incoming velocity

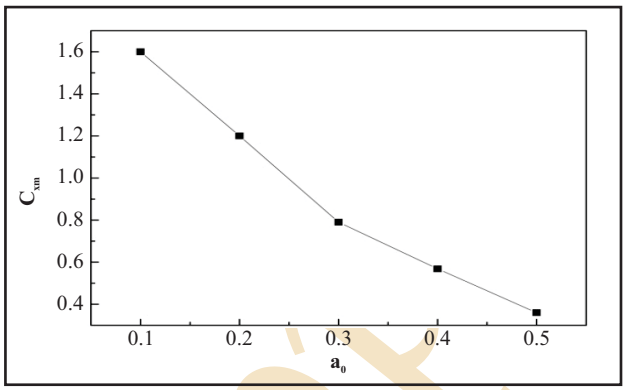

(a) Average thrust coefficient

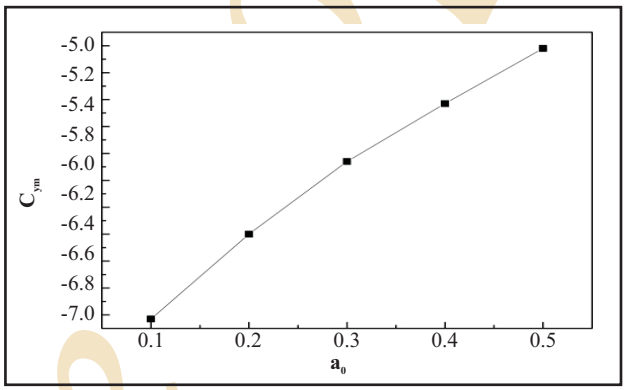

(b) Average lateral force coefficient

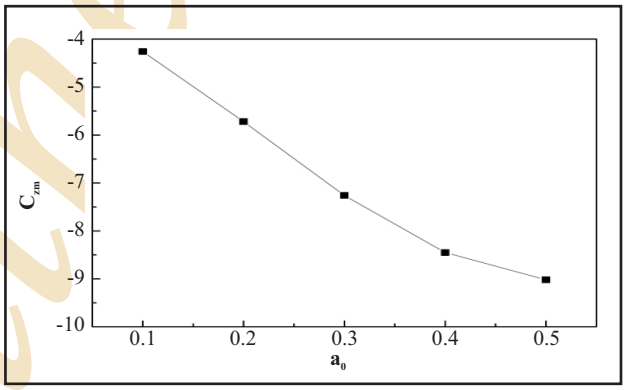

(c) Average lift coefficient

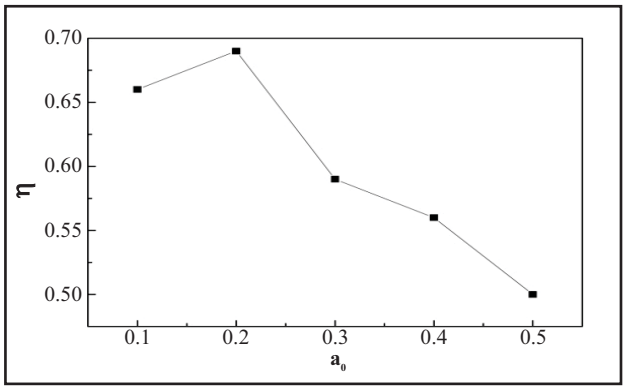

(d) Efficiency

Fig. 18 : Flexure amplitude analysis for the flexible pectoral fin

$\phi_{LC} = \phi_{LA} = 35^{\circ}$, $\phi_{FEA} = \phi_{FEC} = \phi_{FLC} = \phi_{FLA} = 45^{\circ}$, $\Delta\phi_{FE} = \Delta\phi_{FL} = 60^{\circ}$, $f = 0.4$ Hz and $a_0 = 0.1$. The hydrodynamic coefficients during one period is shown in Fig. 13.

After deformation was added, the hydrodynamic coefficients of flexible fin showed same variation trend as there was one of the rigid fin only with difference of variation amplitude. Fig. 14, 15 and 16 showed the evolution of Wy, Wz and Wx in 3-dof motion of flexible pectoral fin during one period respectively.

Fig. 14 denotes that during the motion of flexible pectoral fin, the shedding direction for Wy of flexible fin was same as one of the rigid fin. However, under the effect of flexibility, the shedding time was delayed and shed wake vortices stayed longer time near the fin. As shown in Fig. 15, as compared to rigid fin, the developing and shedding of flexible fin were more obvious and due to flexibility, shed wake vortices took longer time near the fin. Digital visualization of Wz, showed that at same range of contour levels, the amount of wake vortices increased, which led to the increase of the lift (Fig. 13c). Fig. 16, reveals that due to fluid viscosity the shed Wx stayed near the edge of the flexible fin at first, and then gradually dissipated outward as the motion of the fin.

Hydrodynamic comparisons between rigid and flexible pectoral fins : Fig. 17 shows the hydrodynamic performance of rigid and flexible pectoral fins with increase in the incoming velocity in case of $\phi_{LC} = \phi_{LA} = 35^{\circ}$, $\phi_{FEA} = \phi_{FEC} = \phi_{FLC} = \phi_{FLA} = 45^{\circ}$, $\Delta\phi_{FE} = \Delta\phi_{FL} = 60^{\circ}$, $f = 0.4$ Hz and $a_0 = 0.1$. The range of the incoming velocity for computation was $U = 1C \sim 9C$.

Fig. 17 reveals that the variation trend of average hydrodynamic force for both the rigid and flexible fin was basically consistent. As evident from Fig. 17(a) for low incoming velocity, the thrust of flexible fin was smaller than one of the rigid fin and compared to rigid fin, the thrust decreasing of the flexible fin was smaller as the speed increased. However, for high incoming velocity, the thrust of the flexible fin was larger than one of the rigid fin. Fig. 17(b) and 17(c) show as compared to the rigid fin, the smaller lateral force and larger lift were produced by the flexible fin. As revealed from Fig. 17(d) for low incoming velocity, the efficiency of the flexible fin was obviously higher than one of the rigid fin. However, the efficiency of the flexible fin was obviously lower than one of the rigid fin for high incoming velocity. Above analysis shows that the hydrodynamic performance of the flexible fin was better than that of the rigid fin for low incoming velocity, however opposite situation occured for high incoming velocity.

Effect of the flexure amplitude : In this section, the impact of flexure amplitude on the hydrodynamic performance was studied. With the parameters of $U = 4C$, $\phi_{LC} = \phi_{LA} = 35^{\circ}$, $\phi_{FEA} = \phi_{FEC} = \phi_{FLC} = \phi_{FLA} = 45^{\circ}$, $\Delta\phi_{FE} = \Delta\phi_{FL} = 60^{\circ}$ and $f = 0.4$ Hz, the hydrodynamic performance of rigid and flexible pectoral fins are shown in Fig. 18 for different flexure amplitude $a_0 = 0.1$ - 0.5.

With the increase of flexure amplitude increased, the average thrust and average lateral force decreased and the average lift increased. The efficiency increased with increase in the flexure amplitude at first and showed peak point at $a_0 = 0.2$ and after that it rapidly decreased.

Conclusions : The following conclusions can be drawn based on the foregoing account :

(a) The CFD method adopted in this paper can simulate the unsteady motion of the pectoral fin quite well.

(b) After analyzing the hydrodynamic performance caused by different parameters, we can get the optimal U, ϕ_{FLA} and ϕ_{FL} for the pectoral fin: $U = 4C$, $\phi_{FLA} = 45^{\circ}$ and $\Delta\phi_{FL} = 60^{\circ}$.

(c) Wake vortices are shed from two edges of the fin and fin tip and convect downstream and in y direction. Due to the periodicity variation of the wake vortex shedding, twice periodicity variations of the thrust occur during one period. Influenced by flapping motion, the lateral force has two peak points and stronger lift reflection is produced.

(d) The hydrodynamic coefficients of the flexible fin have the same variation trend like that of the rigid fin. Because of its influence by the flexibility, the shedding time is delayed and shed wake vortices stay longer time near the fin, difference of the variation amplitude occurs.

(e) The hydrodynamic performance of the flexible fin is better than that of the rigid fin for low incoming velocity. However, the opposite situation occurs for high incoming velocity.

(f) With the increase of flexure amplitude, the average thrust and average lateral force decrease and the average lift increases. The efficiency decreases after reaching the peak at $a_0 = 0.2$.

Conflict of Interests : The authors declare that there is no conflict of interests regarding the publication of this paper.

Acknowledgment

This work is supported by the National Natural Science Foundation of China (Grant No. 51479039).

References

Azuma, A.: The biokinetics of flying and swimming. Tokyo, Springer (1992).

Drucker, E.G. and G.V. Lauder: Locomotor forces on a swimming fish: three-dimensional vortex wake dynamics quantified using digital particle image velocimetry. *J. Exp. Biol.*, **202**, 2393-2412 (1999).

Gibb, A.C., B.C. Jayne and G.V. Lauder: Kinematics of pectoral fin locomotion in the bluegill sunfish lepomis mecrochirus. *J. Exper. Biol.*, **189**, 133-161 (1994).

Kato, N.: Body form locomotion and foraging in aquatic vertebrates. *Ameri. Zoologist*, **24**, 107-120 (1984).

Kato, N.: Locomotion by mechanical pectoral fins. *J. Mar. Sci. Technol.*, **3**, 113-121 (1998).

Kato, N. : Hydrodynamic characteristics of a mechanical pectoral fin. *J. Fluids Engg.*, **121**, 605-613 (1999).

Kato, N.: Control performance in the horizontal plane of a fish robot with mechanical pectoral fins. *IEEE J. Oce. Engg.*, **25**, 121-129 (2000).

Kato, N., Y. Ando and T. Shigetomi: Precision maneuvering of underwater robot by mechanical pectoral fins. International Symposium on Underwater Technology, pp. 303-310 (2004).

Kato, N. and M. Furushima: Pectoral fin model for maneuver for underwater vehicles. Proc. 1996 IEEE Symp. Autonomous Underwater Vehicle Technology, pp. 49-56 (1996).

Kato, N. and D.M. Lane: Coordinated control of multiple manipulators in underwater robots. Proc. 1996 IEEE Int. Conf. Robotics and Automation. 28 April 1996, Minneapolis, MN, pp. 2505-2510 (1996).

Su, Y.M., Q.M. Cao and W.C. Lai: Analysis of the hydrodynamics of a pectoral fin propulsor. *J. Harbin Engg. Univ.*, **28**, 727-733 (2007).

Su, Y.M., Z.L. Wang, X. Zhang and B.J. Guo: Numerical simulation for hydrodynamic characteristics of a bionic flapping hydrofoil. *China Ocean Engineering*, **26**, 291-304 (2012).

Wang, Z.L., Y.M. Su and L. Yang : Hydrodynamic analysis of the pectoral-fins in viscous flows. *Chin. J. Hydrodyn.*, **24**, 141-149 (2009).

Westneat, M.W. and J.A. Walker: Applied aspects of mechanical design, behavior, and performance of pectoral fin swimming in fishes. Proc. Special Session on Bio-Engineering Research Related to Autonomous Underwater Vehicles. 10th Intern. Symp. Unmanned Untethered Submersible Technology, pp. 153-165 (1997).

Zhang, X., Y.M. Su and Z.L. Wang: Numerical simulation of the hydrodynamic performance of an unsymmetrical flapping caudal fin. *J. Hydrodyn.*, **24**, 354-362 (2012).